From $V_8Ga_{36.9}Zn_{4.1}$ and $Cr_8Ga_{29.8}Zn_{11.2}$ to $Mn_8Ga_{27.4}Zn_{13.6}$: A Remarkable Onset of Zn-Cluster Formation in an Intermetallic Framework

Per Viklund,[b] Christer Svensson,[b] Steve Hull,[c] Sergei I. Simak,[d] Pedro Berastegui,[a] and Ulrich Häußermann*[a]

Abstract: The series of isotypic compounds $V_8Ga_{41} \rightarrow V_8Ga_{36.9}Zn_{4.1} \rightarrow Cr_8Ga_{29.8}Zn_{11.2} \rightarrow Mn_8Ga_{27.4}Zn_{13.6}$ with the V_8Ga_{41} structure type (space group $R\bar{3}$, $Z = 3$) was prepared and structurally characterised by X-ray diffraction experiments (V_8Ga_{41}: a = 13.9351(5), c = 14.8828(12); $V_8Ga_{36.9}Zn_{4.1}$: a = 13.9244(7), c = 14.8660(9); $Cr_8Ga_{29.8}Zn_{11.2}$: a = 13.7153(5), c = 14.6872(9); $Mn_8Ga_{27.4}Zn_{13.6}$: a = 13.6033(6), c = 14.6058(16)). The site occupancies of the ternary compounds were refined from neutron powder-diffraction data and exposed a startling segregation of Zn and Ga, which finally resulted in the formation of separated Zn_{13} cluster entities—corresponding to almost ideal centred cuboctahedra or small pieces of fcc metal–in the Mn compound, which has the highest Zn content in the series. The homogeneity ranges of the underlying phases $T_8Ga_{41-x}Zn_x$ were determined to be $0 < x < 4.1(3)$, $8.7(3) < x < 11.2(3)$ and $13.6(4) < x < 16.5(3)$ for T = V, Cr and Mn, respectively. The different ranges of composition of the phases reflect the requirement of an optimum electron concentration for a stable V_8Ga_{41}-type structure, which is in the narrow range between 159 and 165 electrons per formula unit. First-principles electronic-structure calculations could explain this fact by the occurrence of a pseudo gap in the density of states at which the Fermi level is put for this particular electron concentration. Furthermore the nature of the Zn/Ga segregation was revealed: T–Zn interactions were found to be considerably weaker than those for T–Ga. This places the Zn atoms as far as possible from the T atoms, thus leading to the formation of cuboctahedral Zn_{13} entities.

Keywords: cluster compounds · density functional calculations · intermetallic phases · structure elucidation · zinc

Introduction

The element Zn is not particularly known for its cluster chemistry. The atomic (closed shell) electron configuration $4s^2$ permits only weak van der Waals bonding interactions between Zn atoms in the dimer and in small sized clusters, which change into metallic bonding when the cluster size increases.[1] Then the gap between molecular orbitals that arises from the atomic s and p valence orbitals closes (s–p mixing), and the occupied states highest in energy turn successively from being s–s antibonding to p–p bonding. However, due to the rather large separation of the atomic 4s and 4p states (4 eV[2]), the stabilising mechanism of s–p mixing is not very effective until large cluster sizes are reached. In the elemental structure of Zn (infinitely large cluster), s and p based states (bands) finally overlap to a considerable extent. It was found that the large c/a ratio in hcp-Zn ($c/a = 1.856$ compared with 1.633 for ideal close packing) is due to an optimisation of s–p band mixing.[3] As a consequence Zn clusters are extremely rare as molecular entities, to our knowledge the only reported example is a Zn_4 tetrahedral cluster hosted in the cage of zeolite X[4]. Moreover, in solid state arrays of intermetallic Zn compounds, Zn atoms form extended network structures rather than clusters.[5]

Against this background, we recently reported on the compound $Mn_8Ga_{27.4}Zn_{13.6}$, in which we observed a remarkably clear difference in the site preferences of Zn and Ga, which led to the formation of separated cuboctahedral Zn_{13} cluster entities.[6] These clusters correspond to small volumes of close-packed metal that are interspersed in a primitive cubic host structure formed by the Mn and Ga atoms. The average atomic bond length in a Zn_{13} cluster coincides with

[a] Dr. U. Häußermann, Dr. P. Berastegui
Department of Inorganic Chemistry
Stockholm University, 10691 Stockholm (Sweden)
Fax: (+46) 8 152187
E-mail: ulrich@inorg.su.se

[b] P. Viklund, Dr. C. Svensson
Department of Inorganic Chemistry 2
Lund University, 22100 Lund (Sweden)

[c] Dr. S. Hull
ISIS Facility, Rutherford Appleton Laboratory
Chilton, Didcot, Oxford, OX11 0QX (UK)

[d] Dr. S. I. Simak
Department of Applied Physics
Chalmers University of Technology and Göteborg University
1296 Göteborg (Sweden)

  0947-6539/01/0723-5143 $ 17.50+.50/0

the average nearest-neighbour distance in hcp elemental Zn. At first sight this result is surprising: Zn and Ga are neighbours in the periodic table and have a comparable size (the atomic volumes extracted from the elemental structures are 15.21 Å^3 and 19.57 Å^3 for Zn and Ga, respectively) and electronegativity (1.7 and 1.8 for Zn and Ga, respectively, on the Allred–Rochow scale). Thus, rather than the observed segregation of Zn and Ga, one would expect substitutional disorder of those elements at the sites of the intermetallic framework surrounding the Mn atoms.

In the present work we investigate in detail the driving force of the startling Zn-cluster formation in $Mn_8Ga_{27.4}Zn_{13.6}$. We synthesised the isotypic compounds $V_8Ga_{36.9}Zn_{4.1}$ and $Cr_8Ga_{29.8}Zn_{11.2}$, and thus established the compound series $V_8Ga_{41} \rightarrow V_8Ga_{36.9}Zn_{4.1} \rightarrow Cr_8Ga_{29.8}Zn_{11.2} \rightarrow Mn_8Ga_{27.4}Zn_{13.6}$. Within this series, Zn cluster formation can be studied from the onset (with respect to the known parent compound V_8Ga_{41}[7]) to its full expression in $Mn_8Ga_{27.4}Zn_{13.6}$. We determined the crystal structure of these compounds by combining X-ray and neutron diffraction experiments, and analysed their electronic structure, which was obtained from ab initio calculations.

Results and Discussion

The parent V_8Ga_{41} structure type: In the rhombohedral structure of V_8Ga_{41},[7] V atoms and Ga atoms occupy two and nine different sites, respectively; this yields a total of 147 atoms in the hexagonal unit cell. The V atoms appear to be homogeneously distributed in a matrix of Ga atoms and are separated from each other by the largest distance possible. As a consequence, V atoms have only Ga atoms as nearest neighbours. The two different V atoms have the same kind of 10-vertex coordination polyhedron. These VGa_{10} units represent a hybrid composed of one half of a cube, $VGa_{8/2}$, and one half of an icosahedron, $VGa_{12/2}$, as shown in Figure 1a. To build the V_8Ga_{41} structure, the VGa_{10} polyhedra exclusively share corners and are arranged in such a way that one triangular face of each polyhedron is at the same time part of a cuboctahedron, which is centred by an additional Ga atom (Figure 1b). Thus, such a cuboctahedron is defined by eight VGa_{10} units, which yields the stoichiometry $Ga(VGa_{10/2})_8 = V_8Ga_{41}$ for this compound. This ensemble of eight VGa_{10} hybrid polyhedra joining into a cuboctahedron, $Ga(VGa_{3/2}Ga_7)_8$ (Figure 1c), can also be considered as a three-shell building block, $[GaGa_{12}][V_8][Ga_{56}]$, as depicted in Figure 1d. The surface consisting of 56 Ga atoms has the shape of a (slightly distorted) cube. At the centre of this supercube is located the cuboctahedron surrounded by eight V atoms, which are arranged as a cube that has the same orientation as the outer (super)cube. In the hexagonal unit cell of V_8Ga_{41}, supercubes are connected via the corner-sharing VGa_{10} polyhedra (Figure 1e) and aligned along a body diagonal (Figure 1f). The content of three supercubes corresponds to the content of the hexagonal unit cell of the rhombohedral structure, and the shape and volume of a supercube are equivalent to the primitive rhombohedral cell, although with a different orientation.

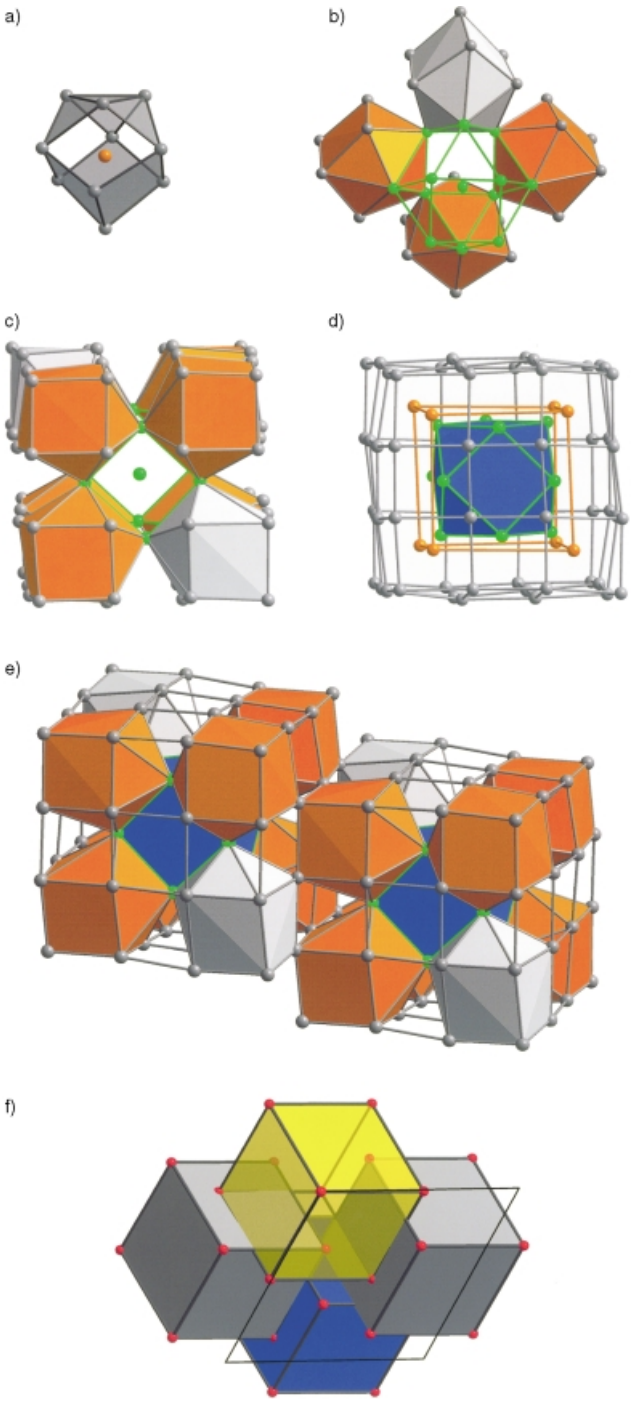

Figure 1. Description of the V_8Ga_{41} structure. a) The coordination polyhedron of the V atoms is a hybrid consisting of one half of a cube (lower part) and one half on an icosahedron (upper part). b) Eight corner-sharing VGa_{10} hybrid polyhedra define a cuboctahedron (only four of them are shown for clarity). This cuboctahedron has the site symmetry $\bar{3}(S_6)$. The two different polyhedron colours, orange and grey, distinguish the two crystallographically different V atoms in the structure. There are two grey polyhedra along the $\bar{3}$ rotation axis of the cuboctahedron and six orange coloured ones around it. c) The ensemble of eight VGa_{10} hybrid polyhedra joining into a cuboctahedron represents a supercube building block. d) The three shells of the supercube building block: the inner shell represents a centred $GaGa_{12}$ cuboctahedron (green/blue), the second shell corresponds to a cube of eight V atoms (orange) and the outer shell to a cube with 56 Ga atoms (grey). e) Supercubes are linked via corner sharing VGa_{10} polyhedra. f) The arrangement of supercube building units in the hexagonal unit cell of V_8Ga_{41}. The supercubes are aligned along the body diagonal running through the two grey VGa_{10} polyhedra.

0947-6539/01/0723-5144 $ 17.50+.50/0 *Chem. Eur. J.* **2001**, *7*, No. 23

The ternary compounds $V_8Ga_{29.1}Zn_{4.1}$, $Cr_8Ga_{29.8}Zn_{11.2}$ and $Mn_8Ga_{27.4}Zn_{13.6}$: The compound V_8Ga_{41} forms from the reaction of the elements by using a large excess of Ga. By employing Zn/Ga melts as a reaction medium, it is possible to exchange a small amount of Ga for Zn in V_8Ga_{41} until a limiting composition $V_8Ga_{29.1}Zn_{4.1}$ is reached. The substitution is accompanied by a small decrease in the lattice parameters. Likewise the phases $Cr_8Ga_{41-x}Zn_x$ and $Mn_8Ga_{41-x}Zn_x$ with the same underlying V_8Ga_{41} structure can be prepared. Table 1 summarises the compositional stability ranges obtained for all three phases T_8E_{41} (T = V, Cr, Mn; E = Zn/Ga). Two important observations can be made. Firstly, the homogeneity ranges are rather narrow and, secondly, the Zn content of the phases is dependent on the transition metal T: the more electron-rich T, the more Zn is incorporated in the corresponding phase T_8E_{41}. As a consequence, the electron count or valence-electron concentration (VEC, number of valence electrons per formula unit) attains a very similar value (or rather a range of values) for all three phases, provided Zn only contributes to bonding by its 4s electrons. This strongly suggests that VEC plays a decisive role for the stability of those phases, which reminds us of the classic Hume–Rothery phases in the system Cu–Zn, in which electron concentration defines the stability ranges of the different brass modifications. The results obtained so far raise the following questions: Why and how is VEC influencing the stability and thus the homogeneity ranges of the investigated phases T_8E_{41}? How is Zn distributed at the Ga sites of the parent V_8Ga_{41} structure type? How is the crystal structure of V_8Ga_{41} affected by the increasing amount of incorporated Zn when T changes from V to Mn?

In order to answer the latter questions we redetermined the crystal structure of V_8Ga_{41} and performed a combined X-ray and neutron-diffraction study on the ternary compounds $V_8Ga_{36.9}Zn_{4.1}$, $Cr_8Ga_{29.8}Zn_{11.2}$ and $Mn_8Ga_{27.4}Zn_{13.6}$[6] (see Experimental Section for details). In particular, each ternary sample was analysed in the following steps: i) verification of the composition by Energy-Dispersive X-ray (EDX) analyses, ii) determination of the lattice parameters from X-ray Guinier powder diagrams; iii) refinement of the atomic position parameters from X-ray single crystal diffraction data, iv) refinement of the Zn/Ga site occupancies from neutron powder diffraction data. X-ray diffraction studies are unable to discriminate between Zn ($Z = 30$) and Ga ($Z = 31$), whereas the neutron scattering lengths of those elements differ by about 20%. The results from the X-ray and neutron data refinements are collected and compared in Tables 2 and 3 (lattice parameters) and Tables 4 to 7 (atomic position

Table 1. Homogeneity ranges of the phases T_8Ga_{41-x} (T = V, Cr, Mn). The compositions were obtained from EDX analyses and the lattice parameters from X-ray powder data.

	V_8Ga_{41}	$V_8Ga_{36.9(3)}Zn_{4.1(3)}$	$Cr_8Ga_{32.3(3)}Zn_{8.7(3)}$	$Cr_8Ga_{29.8(3)}Zn_{11.2(3)}$	$Mn_8Ga_{27.4(4)}Zn_{13.6(4)}$	$Mn_8Ga_{24.5(3)}Zn_{16.5(3)}$
a [Å]	13.9351(5)	13.9244(7)	13.7235(5)	13.7153(5)	13.6033(6)	13.5893(6)
c [Å]	14.8828(12)	14.8660(9)	14.6846(9)	14.6872(9)	14.6058(16)	14.5831(18)
V [Å^3]	2502.9(2)	2496.2(2)	2395.1(2)	2392.7(2)	2340.7(3)	2332.2(3)
VEC [e/f.u.]	163	158.9	162.3	159.8	165.4	162.5

Table 2. X-ray single-crystal refinement data for the compounds V_8Ga_{41}, $V_8Ga_{36.9}Zn_{4.1}$, $Cr_8Ga_{9.8}Zn_{11.2}$ and $Mn_8Ga_{27.4}Zn_{13.6}$. The listed compositions were obtained from EDX analyses and the lattice parameters from X-ray powder data.

Composition	V_8Ga_4	$V_8Ga_{36.9(3)}Zn_{4.1(3)}$	$Cr_8Ga_{29.8(2)}Zn_{11.2(3)}$	$Mn_8Ga_{27.4(4)}Zn_{13.6(4)}$
crystal system	trigonal	trigonal	trigonal	trigonal
space group	$R\bar{3}$ (No. 148)	$R\bar{3}$ (No. 148)	$R\bar{3}$ (No. 148)	$R\bar{3}$ (No. 148)
a [Å]	13.9351(5)	13.9244(7)	13.7153(5)	13.6033(6)
c [Å]	14.8828(12)	14.8660(9)	14.6872(9)	14.6058(16)
V [Å^3]	2502.9(2)	2496.2(2)	2392.7(2)	2340.7(3)
Z	3	3	3	3
ρ_{calcd} [g cm^{-1}]	6.621	6.500	6.715	6.889
crystal size [μm^3]	75 × 75 × 60	50 × 50 × 50	63 × 63 × 63	87 × 87 × 75
transmission (max:min)	1.16	1.70	1.77	2.9
μ [mm^{-1}]	35.06	34.45	35.47	36.49
2θ range hkl	4.3–60.0	4.4–63.3	4.4–63.3	4.4–110.6
index range hkl	$-19 \le h \le 19$	$-19 \le h \le 14$	$-20 \le h \le 15$	$-31 \le h \le 30$
	$-19 \le h \le 14$	$-19 \le k \le 20$	$-20 \le k \le 19$	$-29 \le k \le 24$
	$-20 \le h \le 19$	$-21 \le l \le 21$	$-21 \le l \le 21$	$-32 \le l \le 32$
total no. reflections	13577	8460	8047	31809
independent reflections	996, 498	1752	1684	6678
R_{int}	0.0493, 0.0787	0.0908	0.0493	0.0622
reflections with $I > 2\sigma(I)$	786	942	1254	4737
final R indices [$I > 2\sigma(I)$]	$R_1 = 0.0380$	$R_1 = 0.0450$	$R_1 = 0.0324$	$R_1 = 0.0383$
	$wR_2 = 0.0721$	$wR_2 = 0.0869$	$wR_2 = 0.0677$	$wR_2 = 0.0809$
R indices (all data)	$R_1 = 0.0655$	$R_1 = 0.1136$	$R_1 = 0.0515$	$R_1 = 0.0677$
	$wR_2 = 0.0741$	$wR_2 = 0.1003$	$wR_2 = 0.0716$	$wR_2 = 0.0932$
extinction coefficient	0.00060(2)		0.00063(2)	0.00321(7)
largest diff. peak/hole [eÅ^{-3}]	1.703/−1.542	2.428/−1.889	1.305/−1.153	2.376/−2.733

$R_1 = \Sigma \| F_o | - | F_c \| / \Sigma | F_o |$. $wR_2 = (\Sigma[w(F_o^2 - F_c^2)^2]) / (\Sigma[w(F_o^2)^2])$; $w = 1/[\sigma^2(F_o^2) + (aP)^2 + bP]$ and $P = (F_o^2 + F_c^2)/3$; V_8Ga_{41} ($a = 0.0362$, $b = 0$); $V_8Ga_{36.9(3)}Zn_{4.1(3)}$ (a = 0.00386, b = 0); $Cr_8Ga_{29.8(3)}Zn_{11.2(3)}$ ($a = 0.0340$, $b = 0$); $Mn_8Ga_{27.4(4)}Zn_{13.6(4)}$ ($a = 0.0433$, $b = 1.97$).

Table 3. Neutron powder refinement data for the compounds $V_8Ga_{36.9}Zn_{4.1}$, $Cr_8Ga_{29.8}Zn_{11.2}$ and $Mn_8Ga_{27.4}Zn_{13.6}$. The listed compositions correspond to the refined Zn/Ga site occupancies. The total composition for the V compound was constrained.

Composition	$V_8Ga_{37.0}Zn_{4.0}$	$Cr_8Ga_{29.7(3)}Zn_{11.3(3)}$	$Mn_8Ga_{27.4(1)}Zn_{13.6(1)}$
a [Å]	13.9228(2)	13.7171(1)	13.6059(1)
c [Å]	14.8674(3)	14.6867(1)	14.6063(2)
V [Å 3]	2495.9(1)	2393.2(4)	2341.7(1)
no. of reflns	3021	3288	3687
no. of ref. param	68	53	38
R_p	0.0285	0.0249	0.0452
R_{wp}	0.0175	0.0157	0.0216
R_{bragg}	0.0326	0.0272	0.0438
χ^2	3.78	2.5	1.982

$R_p = \Sigma|y_{oi} - y_{ci}|/\Sigma|y_{oi}|$; $R_{wp} = (\Sigma w|y_{oi} - y_{ci}|^2/\Sigma w|y_{oi}|^2)^{0.5}$

Table 4. Atomic position parameters (standardised with the program Structure Tidy[28]), site occupancies, and isotropic thermal displacement parameters for V_8Ga_{41}. Values in italics refer to the original structure determination.[7] U_{eq} ($\times 10^4$ Å^2) is defined as one third of the trace of the orthogonalised U_{ij} tensor.

Atom	Site	x	y	z	s.o.f.	U_{eq}
T1	18f	0.0380(1)	0.3569(1)	0.0679(1)	1 V	40(3)
		0.0377(1)	*0.3567(1)*	*0.0680(1)*		*49(7)*
T2	6c	0	0	0.1861(2)	1 V	41(5)
		0	*0*	*0.1860(1)*		*46(8)*
Ea1	18f	0.0132(1)	0.1699(1)	0.1137(1)	1 Ga	104(3)
		0.0132(1)	*0.1698(1)*	*0.1136(1)*		*89(6)*
Ea2	18f	0.1827(1)	0.1822(1)	0.2154(1)	1 Ga	98(3)
		0.1832(1)	*0.1824(1)*	*0.2154(1)*		*91(6)*
Ea3	18f	0.3195(1)	0.0092(1)	0.2328(1)	1 Ga	97(3)
		0.3196(3)	*0.0094(1)*	*0.2330(3)*		*88(6)*
Ea4	18f	0.3188(1)	0.1362(1)	0.0063(1)	1 Ga	93(3)
		0.3187(1)	*0.1360(1)*	*0.0062(1)*		*83(5)*
Ea5	9e	0.5	0	0	1 Ga	102(4)
		0.5	*0*	*0*		*92(8)*
Ea6	3a	0	0	0	1 Ga	139(6)
		0	*0*	*0*		*117(1)*
Eb1	18f	0.1236(1)	0.0081(1)	0.3351(1)	1 Ga	168(3)
		0.1235(1)	*0.0081(1)*	*0.3353(1)*		*146(6)*
Eb2	18f	0.2219(1)	0.4239(1)	0.1628(1)	1 Ga	149(3)
		0.2217(1)	*0.4241(1)*	*0.1632(1)*		*122(6)*
Eb3	3b	0	0	0.5	1 Ga	114(6)
		0	*0*	*0.5*		*99(9)*

parameters and site occupancies). In the case of binary V_8Ga_{41}, our structural data are compared with the literature data by Girgis et al.[7] The results of the two structure determinations deviate just slightly (Table 4). Also, the X-ray and neutron diffraction refinement results are in very good agreement, apart from the V atom position parameters in $V_8Ga_{36.9}Zn_{4.1}$, which cannot be refined precisely from neutron diffraction data since the neutron scattering length of V is virtually zero. Further, constraints for the isotropic thermal-displacement factors had to be introduced into the Rietveld refinement of the neutron diffraction data for $V_8Ga_{36.9}Zn_{4.1}$ and $Mn_8Ga_{27.4}Zn_{13.6}$. For the former, the total composition had to be additionally constrained. This, however, is legitimate because for $Cr_8Ga_{29.8}Zn_{11.2}$ and $Mn_8Ga_{27.4}Zn_{13.6}$ the neutron-diffraction-refined total composition matches the result form the EDX analyses well. In the next step, we examined the distribution of Zn in the E atom framework of the ternary phases T_8E_{41} and the accompanied changes in their crystal structures with respect to the binary parent compound V_8Ga_{41}. For this purpose we used the structural parameters obtained from X-ray diffraction studies and the refined site occupancies from neutron diffraction data.

Table 5. Atomic position parameters (standardised with the program Structure Tidy[28]), site occupancies and isotropic thermal displacement parameters for $V_8Ga_{36.9}Zn_{4.1}$. Values in italics and the Zn/Ga site occupancies are results of the Rietveld refinement of the neutron diffraction powder data. U_{eq} ($\times 10^4$ Å^2) is defined as one third of the trace of the orthogonalised U_{ij} tensor.

Atom	Site	x	y	z	s.o.f.	U_{eq}
T1	18f	0.0341(1)	0.3537(1)	0.0686(1)	1 V	55(4)
		0.026(5)	*0.343(5)*	*0.063(3)*		*30*
T2	6c	0	0	0.1813(2)	1 V	42(6)
		0	*0*	*0.1669(7)*		*30*
Ea1	18f	0.0108(1)	0.1690(1)	0.1137(1)	1 Ga	105(3)
		0.0113(3)	*0.1691(3)*	*0.1116(3)*		*89(7)*
Ea2	18f	0.1798(1)	0.1799(1)	0.2172(1)	1 Ga	107(3)
		0.1797(3)	*0.1799(3)*	*0.2170(3)*		*74(7)*
Ea3	18f	0.3199(1)	0.0085(1)	0.2334(1)	1 Ga	96(3)
		0.3197(3)	*0.0090(3)*	*0.2341(3)*		*83(8)*
Ea4	18f	0.3224(1)	0.14011)	0.0049(1)	1 Ga	96(3)
		0.3224(3)	*0.1406(3)*	*0.0046(3)*		*52(6)*
Ea5	9e	0.5	0	0	1 Ga	96(4)
		0.5	*0*	*0*		*72(9)*
Ea6	3a	0	0	0	1 Ga	108(6)
		0	*0*	*0*		*58(15)*
Eb1	18f	0.1204(1)	0.0063(1)	0.3367(1)	0.46(3) Ga	169(3)
		0.1207(3)	*0.0082(3)*	*0.3374(2)*	0.54(3) Zn	*111(4)*
Eb2	18f	0.2214(1)	0.4258(1)	0.1636(1)	0.87(3) Ga	142(3)
		0.2211(3)	*0.4255(3)*	*0.1636(3)*	0.13(3) Zn	*111(4)*
Eb3	3b	0	0	0.5	1 Ga	134(7)
		0	*0*	*0.5*		*56(11)*

Table 6. Atomic position parameters (standardised with the program Structure Tidy[28]), site occupancies and isotropic thermal displacement parameters for $Cr_8Ga_{29.8}Zn_{11.2}$. Values in italics and the Zn/Ga site occupancies are results from the Rietveld refinement of the neutron diffraction powder data. U_{eq} ($\times 10^4$ Å^2) is defined as one third of the trace of the orthogonalised U_{ij} tensor.

Atom	Site	x	y	z	s.o.f.	U_{eq}
T1	18f	0.0301(1)	0.3496(1)	0.0674(1)	1 Cr	48(2)
		0.0309(2)	*0.3513(2)*	*0.0672(2)*		*38(4)*
T2	6c	0	0	0.1813(1)	1 Cr	56(3)
		0	*0*	*0.1814(3)*		*32(7)*
Ea1	18f	0.0090(1)	0.1676(1)	0.1135(1)	1 Ga	92(2)
		0.0090(1)	*0.1674(1)*	*0.1135(1)*		*88(2)*
Ea2	18f	0.1779(1)	0.1784(1)	0.2198(1)	1 Ga	97(2)
		0.1781(1)	*0.1788(1)*	*0.2200(1)*		*72(3)*
Ea3	18f	0.3216(1)	0.0065(1)	0.2321(1)	1 Ga	95(2)
		0.3217(1)	*0.0064(1)*	*0.2322(1)*		*54(3)*
Ea4	18f	0.3251(1)	0.1441(1)	0.0034(1)	1 Ga	93(1)
		0.3249(1)	*0.1446(1)*	*0.0038(1)*		*62(3)*
Ea5	9e	0.5	0	0	1 Ga	104(2)
		0.5	*0*	*0*		*70(4)*
Ea6	3a	0	0	0	0.59(5) Ga	105(3)
		0	*0*	*0*	0.41(5) Zn	*87(2)*
Eb1	18f	0.1188	0.0045	0.3412	1 Zn	133(2)
		0.1184(2)	*0.0042(2)*	*0.3416(1)*		*89(3)*
Eb2	18f	0.2215	0.4286	0.1651	0.19(3) Ga	122(2)
		0.2217(1)	*0.4291(1)*	*0.1644(1)*	0.81(3) Zn	*72(4)*
Eb3	3b	0	0	0.5	0.96(6) Ga	120(3)
		0	*0*	*0.5*	0.04(6) Zn	*79(8)*

0947-6539/01/0723-5146 $ 17.50+.50/0 *Chem. Eur. J.* **2001**, *7*, No. 23

Table 7. Atomic position parameters (standardised with the program Structure Tidy[28]), site occupancies and isotropic thermal displacement parameters for $Mn_8Ga_{27.4}Zn_{13.6}$. Values in italics and the Zn/Ga site occupancies are results from the Rietveld refinement of the neutron diffraction powder data. U_{eq} ($\times 10^4$ Å^2) is defined as one third of the trace of the orthogonalised U_{ij} tensor.

Atom	Site	x	y	z	s.o.f.	U_{eq}
T1	18f	0.02909(2)	0.34819(2)	0.06731(2)	1 Mn	54(1)
		0.0271(3)	*0.3466(3)*	*0.0671(3)*		*49(2)*
T2	6c	0	0	0.18530(2)	1 Mn	56(1)
		0	*0*	*0.1846(5)*		*49(2)*
Ea1	18f	0.00819(2)	0.16520(2)	0.11247(2)	1 Ga	117(1)
		0.0092(2)	*0.1649(2)*	*0.1128(2)*		*49(2)*
Ea2	18f	0.17814(2)	0.17821(2)	0.22089(2)	1 Ga	104(1)
		0.1780(2)	*0.1789(2)*	*0.2201(2)*		*49(2)*
Ea3	18f	0.32224(2)	0.00586(2)	0.23146(2)	1 Ga	102(1)
		0.3212(2)	*0.0051(1)*	*0.2319(2)*		*49(2)*
Ea4	18f	0.32430(2)	0.14474(2)	0.00336(2)	1 Ga	101(1)
		0.3249(2)	*0.1452(2)*	*0.0045(2)*		*49(2)*
Ea5	9e	0.5	0	0	1 Ga	89(1)
		0.5	*0*	*0*		*49(2)*
Ea6	3a	0	0	0	1 Zn	131(1)
		0	*0*	*0*		*66(3)*
Eb1	18f	0.11906(2)	0.00446(2)	0.34394(2)	1 Zn	125(1)
		0.1183(3)	*0.0043(3)*	*0.3447(3)*		*66(3)*
Eb2	18f	0.22135(2)	0.42996(2)	0.16536(2)	1 Zn	120(1)
		0.2217(3)	*0.4289(3)*	*0.1645(3)*		*66(3)*
Eb3	3b	0	0	0.5	0.39(9) Ga	125(1)
		0	*0*	*0.5*	*0.61(9) Zn*	*66(3)*

Variations in the crystal structure: For the following discussion we divide the E atom network into six Ea-type atoms that form the supercube surface and three Eb-type atoms that define the centred cuboctahedron (cf. Figure 1d). Further analysis is focussed on the variations in the coordination polyhedra around T1, T2 and Eb3 ($T1E_{10}$, $T2E_{10}$, $Eb3Eb_{12}$, respectively). The coordination polyhedra occurring in the structure of the four compounds are shown in Figure 2, the distances between the central atoms and polyhedron atoms are compiled in Table 8. The 10-vertex polyhedron around T1 has point symmetry 1(C_1) and consists of the E atoms Ea1-$Ea2$-$Ea3_2$-$Ea4_2$-Ea5-Eb1-Eb_2, whereas the corresponding polyhedron around T2 has point symmetry 3(C_3) and employs the atoms $Ea1_3$-$Ea2_3$-Ea6-$Eb1_3$. The cuboctahedron around Eb3 has point symmetry $\bar{3}$(S_6) and contains two equilateral triangles (site Eb1), which sandwich a six-membered ring of Eb2 atoms. The equilateral triangles are at the same time part of the T2 coordination polyhedra. The rotational axes of the polyhedra around T2 and Eb3 coincide with the *c* direction in the hexagonal unit cell of the rhombohedral crystal structure.

On going from the binary parent compound V_8Ga_{41} to $V_8Ga_{36.9}Zn_{4.1}$, the Zn atoms segregate into the cuboctahedral sites Eb1 and Eb2, but with a different preference (Eb1: 54% Zn/46% Ga; Eb2: 13% Zn/87% Ga). The centre Eb3 of the cuboctahedron remains a pure Ga site. The different preference of Zn for the two cuboctahedral sites is also reflected in the variation of the bond lengths: d(Eb1–Eb1) decreases from 2.89 Å in V_8Ga_{41} to 2.83 Å in $V_8Ga_{36.9}Zn_{4.1}$, whereas d(Eb2–Eb2) changes from 2.94 Å to 2.91 Å. In $Cr_8Ga_{29.8}Zn_{11.2}$, the Eb1 position becomes fully occupied by Zn whereas the site Eb2 consists of 81% Zn and 19% Ga. Additionally the centre of the cuboctahedron starts to get occupied by Zn (4% Zn/96% Ga). Furthermore, we found the position Ea6 to be a mixture of Zn and Ga (41% Zn/59% Ga). This special site corresponds to the high-symmetry Wyckoff site 3a (0,0,0) and is part of the T2 coordination polyhedron. In the supercube description of the V_8Ga_{41} structure type the position Ea6 is located on, those opposite corners of each cube that define the body diagonal along the supercubes are oriented in the unit cell (cf. Figure 1d and f). Finally in $Mn_8Ga_{27.4}Zn_{13.6}$, both sites Eb1 and Eb2 that define the cuboctahedron are exclusively occupied by Zn atoms. This is also the case for the position Ea6, whereas the centre Eb3 of the cuboctahedral clusters represents the only significantly detected randomly occupied atomic position (61% Zn and 39% Ga) in the structure of this compound. As a result, we can arrange the network E sites in the V_8Ga_{41} structure according to their preference for being occupied by Zn: Eb1 > Eb2 > Ea6 > Eb3 ≫ Ea1 to Ea5.

Accompanying the increasing Zn content in the phases T_8E_{41} there are subtle but decisive changes in the framework interatomic distances. The segregation of Zn on the sites Eb1–Eb3 has the important consequence that the bond lengths within the centred cuboctahedron become more and more equal. Their distribution range starts off from 2.89–3.04 Å in binary V_8Ga_{41} and is finally confined between 2.75 and 2.81 Å in $Mn_8Ga_{27.4}Zn_{13.6}$. Interestingly, the average length of 2.79 Å within Eb_{13} entities in the latter compound corresponds exactly to the average nearest-neighbour distance in the elemental structure of hcp-Zn. Figure 3 summarises the change in the bond-length distribution in the cuboctahedral entities Eb_{13} in the investigated compound series. As the Eb_{13} cuboctahedra become more regular, the TE_{10} polyhedra become more and more elongated because the triangles Eb3 that are part of the cuboctahedron "detach" from the adjoined 10-vertex hybrid polyhedra. The successive elongation of the distances Ea–Eb in those polyhedra is especially clearly seen for $T1E_{10}$, where a gap opens in the distance distribution on going from V_8Ga_{41} to $Mn_8Ga_{27.4}Zn_{13.6}$ (Figure 4). As a consequence of the increasing Ea–Eb distances, the T atoms become primarily coordinated by Ea atoms (i.e. the cube part of the 10-vertex hybrid polyhedron, cf. Figure 1a), which again is more clearly seen in the trend of the T1–E lengths compared with the T2–E ones (Figure 5 and Table 8). Concerning the distribution of distances T2–E, we note that d(T2–Ea6)—the Ea6 position is the high-symmetry Wyckoff site 3a, which is situated on the C_3 axis of the 10-vertex polyhedron—is considerably longer than the other distances T2–Ea.

In conclusion, in the compound series $V_8Ga_{41} \rightarrow V_8Ga_{36.9}Zn_{4.1} \rightarrow Cr_8Ga_{29.8}Zn_{11.2} \rightarrow Mn_8Ga_{27.4}Zn_{13.6}$, we observe a clear segregation of Zn and Ga in the intermetallic framework; this leads to a clustering of Zn and finally to the formation of Zn_{13} cuboctahedral entities in the Mn compound that has the highest Zn content. At the same time, the average bond length within these centred cuboctahedra approaches the average nearest-neighbour distance in elemental Zn. Thus, the formed Zn clusters in $Mn_8Ga_{27.4}Zn_{13.6}$ may be regarded as small volumes of fcc metal that are separated by at least 3.93 Å as the shortest distance between Zn atoms belonging to neighbouring cuboctahedra; the distance be-

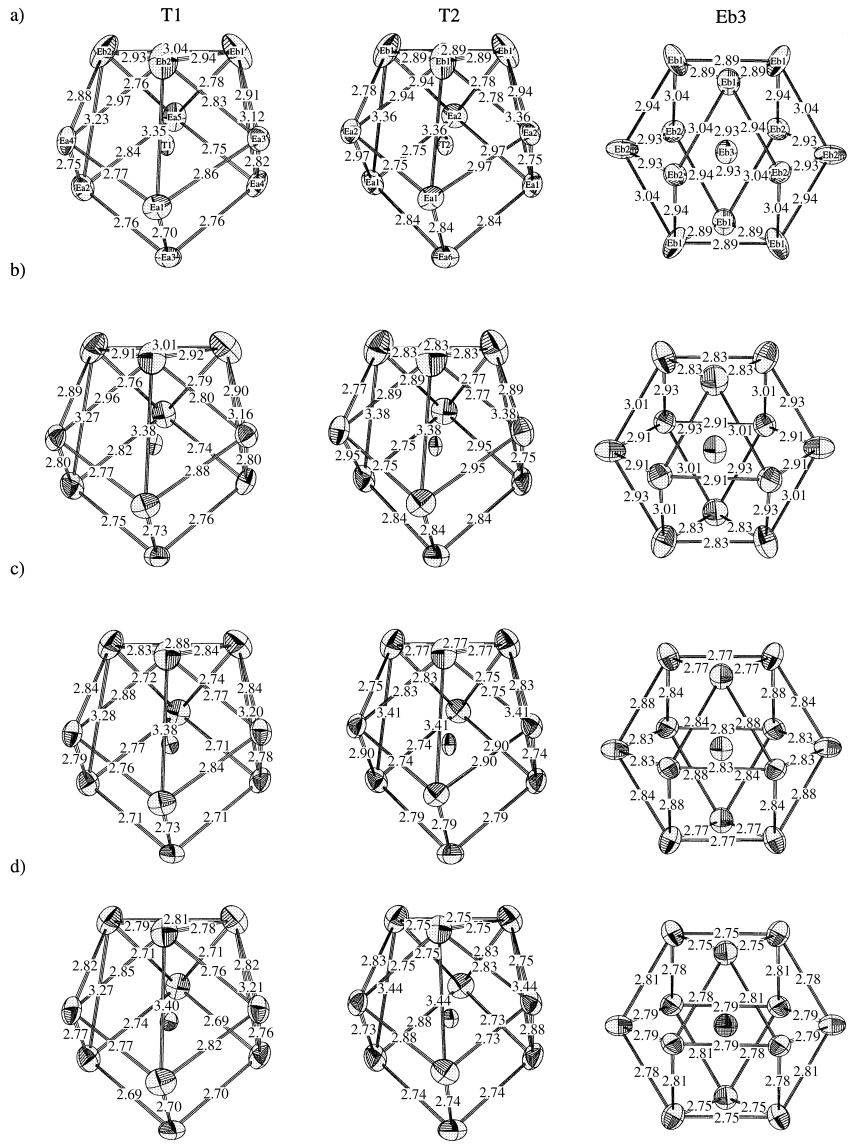

Figure 2. Coordination polyhedra around the two different transition metal sites T1 and T2, and the centre of the cuboctahedron (site Eb3) in the structure of the compounds a) V_8Ga_{41}, b) $V_8Ga_{36.9}Zn_{4.1}$, c) $Cr_8Ga_{29.8}Zn_{11.2}$, d) $Mn_8Ga_{27.4}Zn_{13.6}$. The thermal ellipsoids correspond to the 95% probability level.

tween the centres of the clusters is 9.24 Å. We now turn to the analysis of the electronic structure of the phases T_8E_{41}, which should explain their narrow compositional ranges, suggesting that phase stability is determined by the valence-electron concentration, and further reveal the reason behind the astonishing segregation of Zn and Ga.

Variations in the electronic structure: In Figure 6 we present the density of states (DOS) for the compounds V_8Ga_{41}, $Cr_8Ga_{29.8}Zn_{11.2}$ and $Mn_8Ga_{27.4}Zn_{13.6}$ in their experimentally determined structures (lattice parameters, atomic positions parameters and site occupancies). Those sites exhibiting substitutional disorder were modelled by the virtual-crystal approximation (see Experimental Section for details). Figure 6a shows the total DOS together with the partial DOS of the T and E sites. Figure 6b represents a close-up of the partial DOS curves in which the partial DOS of the E sites is further divided into its Ea and Eb contributions. When focussing first on the electronic structure of the parent compound V_8Ga_{41}, we observe that the DOS at lower energies is dominated by approximately parabolically distributed states that stem from the s – p bands of the Ga atom matrix, which at higher energy are perturbed by the V atom d states.

Table 8. Distances [Å] of the first coordination sphere around the sites T1, T2 and Eb3 in V_8Ga_{41}, $V_8Ga_{36.9}Zn_{4.1}$, $Cr_8Ga_{29.8}Zn_{11.2}$ and $Mn_8Ga_{27.4}Zn_{13.6}$. Standard deviations less than 0.001 Å are not listed.

V_8Ga_{41}			$V_8Ga_{36.9}Zn_{4.1}$			$Cr_8Ga_{29.8}Zn_{11.2}$			$Mn_8Ga_{27.4}Zn_{13.6}$		
T1	Ea5	2.513(2)	T1	Ea3	2.509(2)	T1	Ea1	2.460(1)	T1	Ea3	2.441
	Ea3	2.517(2)		Ea1	2.516(2)		Ea3	2.467		Ea1	2.452
	Ea3	2.540(2)		Ea3	2.521(2)		Ea3	2.481		Ea4	2.456
	Ea1	2.546(2)		Ea5	2.526(2)		Ea4	2.486(1)		Ea3	2.475
	Ea4	2.574(2)		Ea4	2.558(2)		Ea5	2.502		Ea5	2.491
	Ea2	2.595(2)		Ea2	2.581(2)		Ea2	2.529(1)		Ea2	2.500
	Ea4	2.595(2)		Ea4	2.586(2)		Ea4	2.532(1)		Ea4	2.510
	Eb2	2.654(2)		Eb2	2.681(2)		Eb2	2.698(1)		Eb2	2.687
	Eb2	2.690(2)		Eb2	2.721(2)		Eb2	2.740(1)		Eb2	2.744
	Eb1	2.735(2)		Eb1	2.805(2)		Eb1	2.798(1)		Eb1	2.775
T2	Ea1 × 3	2.523(2)	T2	Ea1 × 3	2.494(2)	T2	Ea1 × 3	2.450	T2	Ea1 × 3	2.438
	Ea2 × 3	2.580(1)		Ea2 × 3	2.561(1)		Ea2 × 3	2.508		Ea2 × 3	2.479
	Ea6	2.770(3)		Ea6	2.695(3)		Ea6	2.661(1)		Ea6	2.707
	Eb1 × 3	2.775(3)		Eb1 × 3	2.829(3)		Eb1 × 3	2.842(1)		Eb1 × 3	2.810
Eb3	Eb2 × 6	2.933(2)	Eb3	Eb1 × 6	2.908(1)	Eb3	Eb1 × 6	2.829	Eb3	Eb1 × 6	2.779
	Eb1 × 6	2.968(2)		Eb2 × 6	2.927(1)		Eb2 × 6	2.829		Eb2 × 6	2.790

0947-6539/01/0723-5148 $ 17.50+.50/0 *Chem. Eur. J.* **2001**, *7*, No. 23

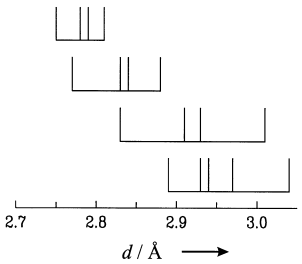

Figure 3. Trend in the distance distribution Eb–Eb within the Eb_{13} cuboctahedral entities in the structure of the compounds V_8Ga_{41} (bottom), $V_8Ga_{36.9}Zn_{4.1}$, $Cr_8Ga_{29.8}Zn_{11.2}$ and $Mn_8Ga_{27.4}Zn_{13.6}$ (top).

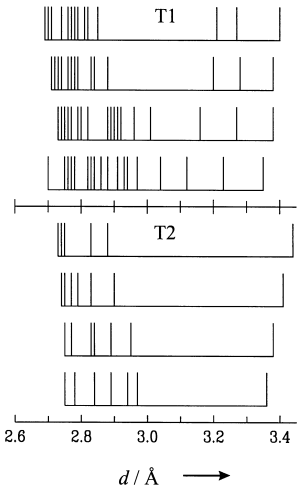

Figure 4. Trend in the distance distribution E–E in the TE_{10} polyhedra (T1 and T2) occurring in the structure of the compounds V_8Ga_{41} (bottom), $V_8Ga_{36.9}Zn_{4.1}$, $Cr_8Ga_{29.8}Zn_{11.2}$ and $Mn_8Ga_{27.4}Zn_{13.6}$ (top).

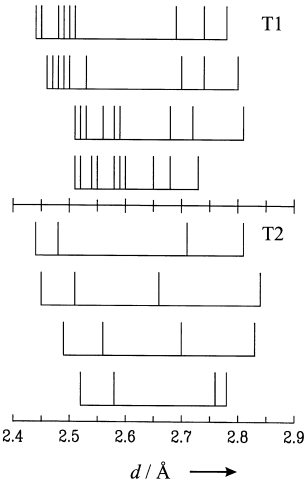

Figure 5. Trend in the distance distributions T1-E and T2-E in the structure of the compounds V_8Ga_{41} (bottom), $V_8Ga_{36.9}Zn_{4.1}$, $Cr_8Ga_{29.8}Zn_{11.2}$ and $Mn_8Ga_{27.4}Zn_{13.6}$ (top).

The strong interaction between V d states and Ga p states (d–p mixing or d–p hybridisation) opens up a broad pseudo gap in the DOS that separates d–p bonding from antibonding states.[8] The occurrence of such a pseudo gap at or close to the Fermi level is a characteristic feature of intermetallic electron compounds, that is, compounds in which the stable crystal structure is mainly controlled by the electron concentration.[9] Below the Fermi level, the V states are confined to a range of about 2 eV (Figure 6b). Interestingly, the distributions of Ea- and Eb-based states differ from each other: it is the partial DOS from the Ea sites that changes shape (i.e. attains a maximum) in the energy range of the V d states with respect to the featureless low-energy region, whereas the distribution of the Eb-site-based states basically remains uninfluenced. Thus, only Ea-type atoms interact strongly with the V atoms. In V_8Ga_{41}, the Fermi level corresponding to a VEC of 163 is slightly above the pseudo gap and enters the d–p antibonding region of electronic states. The effect of the incorporation of a small amount of Zn into this compound immediately becomes clear. A substitution of the more electron-rich Ga for Zn moves the Fermi level towards the centre of the pseudo gap, and the maximum amount of Zn (compositional range border $x = 4.1$) corresponds to the situation where the Fermi level starts to cross the lower energy boundary of the pseudo gap (VEC = 158.9). Thus, a further increase of the amount of incorporated Zn (or equivalently, a further decrease of VEC) becomes unfavourable because d–p bonding states get depopulated.

Turning to $Cr_8Ga_{29.8}Zn_{11.2}$, we firstly notice the occurrence of the Zn d states, which can be considered as bonding inactive, because they are centred far below the Fermi level and are well localised in a narrow range. Further, the Fermi level corresponding to a VEC of 159.8 electrons per formula unit is situated in the centre of the pseudo gap. Thus, compared with the electronic structure of V_8Ga_{41}, the location of the pseudo gap is virtually unchanged, and the compositional stability range of the phase $Cr_8Ga_{41-x}Zn_x$, which conforms to a VEC range of 159.6 - 162.3 (Table 1), is intimately connected with the width of the pseudo gap. Moreover, the trends in the partial DOS of the T, Ea and Eb sites are very similar to the one observed in V_8Ga_{41}; this indicates that the Ea-type atoms interact much more strongly with the T atoms than the Eb ones. However, a careful inspection of the total DOS and partial Cr DOS in the d–p bonding region below the Fermi level reveals the beginning of a splitting of those states into two parts (marked in Figure 6). This splitting becomes rather noticeable in the DOS of $Mn_8Ga_{27.4}Zn_{13.6}$, and it can be clearly seen that just the lower parts of the Mn d levels, centred around −2 eV below the Fermi level, hybridise strongly with the Ea-based states, whereas the upper, more narrow, parts only interact weakly. For the composition $Mn_8Ga_{27.4}Zn_{13.6}$ with VEC = 165.4, which represents the limiting composition with a maximum content of Ga for the phase $Mn_8Ga_{41-x}Zn_x$, the Fermi level is slightly above the pseudo gap. This is comparable to the situation in V_8Ga_{41}. Again, the increase of the Zn content until the maximum concentration $x = 16.5$ reduces VEC and moves the Fermi level towards the centre of the pseudo gap. Yet the preferred sites for Zn, Eb1–Eb3 and Ea6 are completely occupied for $x = 14$, and for compositions above this value Zn has to enter the unfavourable positions Ea1–Ea5. In conclusion, the composition and the homogeneity range of the phases T_8E_{41} are closely linked to the location and the width of the pseudo gap in the DOS, respectively. This pseudo gap is a consequence of strong bonding between T and E atoms, and stable compounds with the V_8Ga_{41} structure type only occur for those elemental compositions that produce an electronic

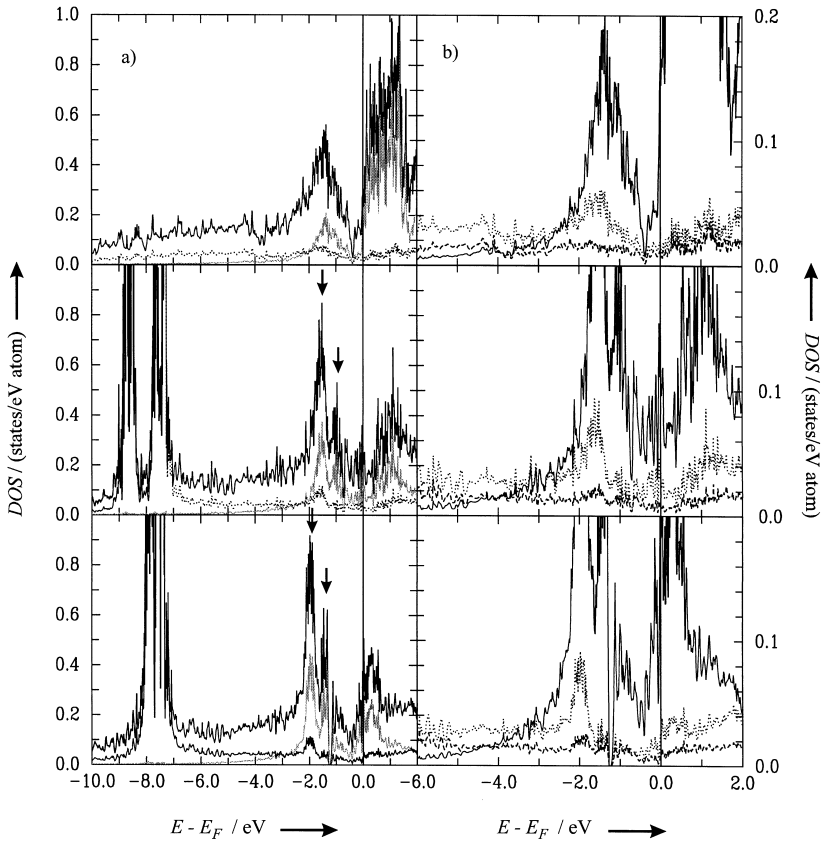

Figure 6. a) Total density of states (DOS; states per eV and atom) together with the T (grey lines) and E partial DOS (dotted lines) for the compounds V_8Ga_{41} (top), $Cr_8Ga_{29.8}Zn_{11.2}$ (middle) and $Mn_8Ga_{27.4}Zn_{13.6}$ (bottom). The arrows mark a splitting of d–p bonded states. b) Close-up of the partial density of states of the T (solid lines), Ea (dotted lines) and Eb (broken lines) sites of the compounds V_8Ga_{41} (top), $Cr_8Ga_{29.8}Zn_{11.2}$ (middle) and $Mn_8Ga_{27.4}Zn_{13.6}$ (bottom).

structure in which the Fermi level is located at, or close to, the pseudo gap. This finding also includes Mo_8Ga_{41}, which is the only other binary representative of the rare V_8Ga_{41} structure type.[10] Since Mo is more electron rich than V, a considerable amount of d–p antibonding states should be occupied in Mo_8Ga_{41}, assuming a rigid band behaviour of the electronic structures of the two binary compounds. However, Mo_8Ga_{41} was reported to be Mo deficient. This deficiency reduces VEC and thus releases the unfavourable bonding situation.

Having explained the decisive role of VEC for structural stability of the investigated phases, we are left with the fundamental question: what is the nature of the different site preferences of Ga and Zn? That is, what is the driving force for the startling clustering of Zn in the framework of the underlying V_8Ga_{41} structure type? For this purpose we compared the density of states of Zn/Ga-ordered $Mn_8Ga_{27.4}Zn_{13.6}$ (experimental site occupancies) with a situation where Zn and Ga atoms occupy all sites E in a completely random way. In this case, the overall E site occupancy has to correspond to 67% Ga/33% Zn in order to fit the total composition. The result is shown in Figure 7. We note that the size and location of the pseudo gap with respect to the Fermi level is the same for the ordered and the disordered structure. However, the decisive difference is the occurrence of a splitting of the d–p bonding states into two parts in the ordered structure which is absent in the disordered one. The DOS of the latter is similar to that of V_8Ga_{41} (cf. Figure 6). Thus, Zn/Ga ordering leads to a splitting of the d–p bonding states which, importantly, puts the T–Ea bonding part of those states at a considerably lower energy with respect to the disordered structure. Since the Ea sites are primarily occupied by Ga atoms T–Ga interactions appear notably stronger than those for T–Zn. This is in accordance with our previous investigation of the compounds $CrGa_4$ and $MnGa_4$ with the $PtHg_4$ structure, where we found that the T–Ga interactions are of a strong covalent nature.[11] As a matter of fact, in some cases (e.g. in $FeGa_3$ and $RuGa_3$) T–Ga interactions can become so strong that instead of a pseudo gap a real band gap is opened at the Fermi level, which leads to semimetallic behaviour.[12] With this finding, we have answered the question raised initially. Zn has in fact no inherent tendency to form clusters. Its segregation into the sites Eb1–Eb3 and the position Ea6 in the structure of the

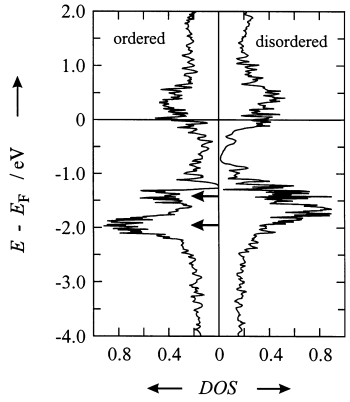

Figure 7. Comparison of the DOS for $Mn_8Ga_{27.4}Zn_{13.6}$ with an ordered and a disordered Zn/Ga distribution. The arrows mark a splitting of d–p bonded states in the ordered variant.

investigated phases T_8E_{41} is a consequence of strong T–Ga and weak T–Zn interactions. The occupation of those sites by Zn ensures that Zn atoms are placed as far as possible from the T atoms and vice versa, Ga atoms become situated as close as possible to the T atoms (cf. Figure 5 and Table 8). The most stable atom arrangement corresponds to a Zn/Ga distribution in which T–Ga bonding interactions are maximised and this leads—but just coincidentally!—to the formation of cuboctahedral Zn_{13} cluster entities.

0947-6539/01/0723-5150 $ 17.50+.50/0 *Chem. Eur. J.* **2001**, *7*, No. 23

Conclusion

This study reports on the series of compounds, $V_8Ga_{41} \rightarrow V_8Ga_{36.9}Zn_{4.1} \rightarrow Cr_8Ga_{29.8}Zn_{11.2} \rightarrow Mn_8Ga_{27.4}Zn_{13.6}$ (V_8Ga_{41} structure type), that was investigated by combined X-ray and neutron-diffraction experiments. Especially, the neutron-diffraction data were used to unequivocally extract the distribution of Zn and Ga atoms in the intermetallic framework. Within this series, a startling clustering of Zn is observed, which, for the Mn compound, culminates in the formation of separated cuboctahedral Zn_{13} entities corresponding to small volumes of close-packed metal. The different composition and the narrow homogeneity range of the underlying phases $T_8Ga_{41-x}Zn_x$ (T = V: $0 < x < 4.1$, T = Cr: $8.7 < x < 11.2$, T = Mn: $13.6 < x < 16.5$) are closely linked to the location and the width of a pseudo gap in the density of electronic states. This pseudo gap is a consequence of strong bonding between T and E atoms, and stable compounds with the V_8Ga_{41} type only occur for those elemental compositions that produce an electronic structure in which the Fermi level is located at, or close to, the pseudo gap. The puzzle of the extraordinary Zn clustering was solved by comparing the density of states of Zn/Ga-ordered and disordered $Mn_8Ga_{27.4}Zn_{13.6}$. It was found that T–Zn interactions are considerably weaker than those for T–Ga; this places the Zn atoms as far as possible from the T atoms. Thus, the different T–E interactions govern a subtle ordering tendency of the chemically similar metals Zn and Ga in a complex intermetallic framework, which, coincidentally, leads to an unusual formation of Zn clusters.

Experimental Section

Synthesis and compositional analysis: The phases T_8E_{41} (T = V, Cr, Mn; E = Zn/Ga) were prepared from mixtures of the pure elements [Cr powder (Goodfellow Metals, >99.4%), Mn powder (Goodfellow Metals, >99.9%), V powder (ABCR, >99.5%), Ga rod (ABCR, >99.9999%) and Zn granules (ABCR, >99.99%)] containing 1 mole equivalent T component and a total amount of 10 to 20 mole equivalents E component with different Zn/Ga ratios. The reactants were pressed into pellets and loaded into quartz ampoules, which were sealed under vacuum (approx. 10^{-4} atm). Ternary samples were heated to 900 °C at a rate of 200 °C h^{-1}, held at this temperature for 24 h, and finally cooled to room temperature at a rate of 10 °C h^{-1}. The heating scheme for the synthesis of binary V_8Ga_{41} had to be modified in order to avoid the formation of V_2Ga_5[13] as the main product. This sample was heated to 850 °C at a rate of 200 °C h^{-1}, annealed for two days at 850 °C, then rapidly cooled to 450 °C, kept at this temperature for seven days and finally cooled to room temperature at a rate of 20 °C h^{-1}. Excess E (Ga/Zn) metal was always dissolved in 4 M HCl and the residues washed with deionised water. All products in the examined systems consisted of shiny, silvery-grey crystals that ranged in size from approximately 100 microns to 1 mm. The ternary phases $T_8Ga_{41-x}Zn_x$ with T = Cr, Mn could also be obtained from stoichiometric mixtures of the elements, however crystal quality and homogeneity of the products were found to be considerably higher when a flux of excess E metal is present. The homogeneity ranges (phase widths) of the systems $T_8Ga_{41-x}Zn_x$ were established from reaction series by employing E melts with varying Zn/Ga ratios. The products were characterised by Guinier powder diagrams (Cu Kα; Si standard) and their composition analysed with the EDX (energy-disperse X-ray) method in a JEOL JSM-840A scanning electron microscope averaging at least ten analyses for each sample. For the Cr and Mn containing systems, mixtures with a Ga/Zn ratio larger than 3 yielded the compounds $CrGa_4$ and $MnGa_4$[11] (with the $PtHg_4$ structure) and virtually no $T_8Ga_{41-x}Zn_x$. Concerning the V systems, the occurrence of a variable amount (depending on the synthesis conditions) of V_2Ga_5 (or $V_2Ga_{5-x}Zn_x$) as by-product was observed in all samples. The result of the homogeneity range studies is compiled in Table 1.

Structure determination:

X-ray investigations: A Huber Guinier G 670 image foil powder camera with monochromatised Cu Kα radiation, was used for the collection of powder diffractograms (at room temperature). Silicon (SICOMILL, Kema Nord, Nobel Industries, Sweden) was used as internal standard. Lattice parameters were obtained from least-squares refinements of the measured and indexed lines of these powder diagrams (program PIRUM[14]). Single crystal intensity data was collected from one crystal from each of the following samples V_8Ga_{41}, $V_8Ga_{36.9(3)}Zn_{4.1(3)}$, $Cr_8Ga_{29.8(3)}Zn_{11.2(3)}$ and $Mn_8Ga_{27.4(4)}Zn_{13.6(4)}$ (EDX determined compositions) on a Siemens SMART CCD three-circle diffractometer system[15] at room temperature with monochromatised Mo Kα radiation (0.71073 Å). The data collection nominally covered a full sphere of reciprocal space. In each case, data were corrected for Lorentzian polarisation,[16] extinction and absorption (assuming a spherical crystal).[17] The space group $R\bar{3}$ was assigned on the basis of the systematic absences and the statistical analysis of the intensity distributions. The structure of $Mn_8Ga_{27.4}Zn_{13.6}$ was solved by direct methods and refined against F^2 by using SHELXTL.[18] The structures of the other compounds were refined by using the atomic position parameters of the Mn compound as a starting model. To prepare the data set of V_8Ga_{41} for refinement, an additional program, Twin Solve,[19] was put into practice due to rotational twinning of the crystal. The choice of a twinned crystal for structure solution and refinement is not preferable, but was made due to the lack of a better crystal than the one selected. The twinning could not be recognised until the later stages of the refinement when there were still residual electron-density peaks that were too large present (>4 e Å^{-1}), and the R_1 value was approximately twice as high as those obtained with the data sets from the crystals of the other systems. The V_8Ga_{41} crystal appeared to consist of two unequally sized individuals, mutually twinned. In the subsequent refinement, both nonoverlapping and overlapping reflections (intensity corrected for the overlap of the minor individual) of the larger individual were used. The refinement proceeded smoothly and converged at satisfying values, comparable to the other compounds. Some details of the single crystal data collections and refinements are listed in Table 2. Atomic position parameters and selected interatomic distances are given in Tables 4–8. Further details of the crystal-structure investigation may be obtained from Fachinformationszentrum Karlsruhe, 76344 Eggenstein-Leopoldshafen, Germany (fax: (+49) 7247-808-666; e-mail: crysdata@fiz-karlsruhe.de) on quoting the depository number CSD-410318 ($Mn_8Ga_{27.4}Zn_{13.6}$), CSD-411900 ($Cr_8Ga_{29.8}Zn_{11.2}$), CSD-411898 ($V_8Ga_{36.9}Zn_{4.1}$) and CSD-411899 (V_8Ga_{41}).

Neutron investigations: Neutron diffraction experiments on $V_8Ga_{36.9(3)}Zn_{4.1(3)}$, $Cr_8Ga_{29.8(3)}Zn_{11.2(3)}$ and $Mn_8Ga_{27.4(4)}Zn_{13.6(4)}$ (EDX-determined compositions) were performed on the Polaris powder diffractometer at the ISIS facility, UK, with the samples encapsulated inside thin-walled vanadium cans. Time-of-flight diffraction data were collected at room temperature by using the backscattering detector bank, which covers the scattering angles $135° < \pm 2\theta < 160°$ and provides data over the d-spacing range $0.5 < d < 3.2$ Å with a resolution $\Delta d d^{-1} = 5 \times 10^{-3}$. Rietveld profile refinements with the normalised diffraction data were performed by using the program GSAS[20]. The $V_8Ga_{36.9}Zn_{4.1}$ sample was found to contain two additional phases, V_2Ga_5[13] with a small amount of Zn incorporated into the structure and—for unknown reasons—cubic VO.[21] A multiphase refinement was performed including eight background parameters, an extinction correction parameter and three profile parameters for each phase [refined weight fractions: $V_8Ga_{36.9}Zn_{4.1}$ (59%), $V_2Ga_{3.8}Zn_{1.2}$ (25%), VO (16%)]. Initial values for the V coordinates were obtained from the single-crystal X-ray diffraction experiment and were constrained with a damping factor in the refinement. Temperature factors for the V atoms were constrained to a fixed value. Due to the large correlation between temperature factors and occupancies, the Zn content was constrained to the value obtained from EDX analyses (approx. 12 Zn atoms in the unit cell), and each Ga site was refined for partial occupancy. The final refinement showed that the Eb1 and Eb2 sites are partially occupied by Zn and, at this point, the temperature factors at these two sites were constrained to have the same value. No indication of Zn occupying the other sites was found. The results of the Rietveld analyses are presented in Tables 3 and 5. The $Cr_8Ga_{29.8}Zn_{11.2}$ sample was single phase and the Zn content could be refined

to a value close to the one obtained from EDX analyses. Partial occupancy was observed at sites Eb2, Eb3 and Ea6. The Eb1 site was found to be fully occupied by Zn. Rietveld refinements were carried out as for the previous sample and included eight background parameters, four profile parameters and an extinction correction. Partial occupancy was refined at each site but Zn was found to occupy the mentioned sites in the structure preferentially. Tables 3 and 6 show the final results of the refinement. Also, the $Mn_8Ga_{27.4}Zn_{13.6}$ sample was single phase. The refined Zn content coincided with the result of the EDX analysis. Rietveld refinements included eight background parameters, four profile parameters and an extinction correction. Due to a strong correlation between temperature factors and occupancies, only two temperature factors, for the Mn and Ga atoms and for the Zn atoms, were refined.[6] The results are presented in Tables 3 and 7.

Electronic structure calculations: The electronic structures of V_8Ga_{41}, $Cr_8Ga_{29.8}Zn_{11.2}$ and $Mn_8Ga_{27.4}Zn_{13.6}$ in their experimentally determined crystal structures (lattice parameters, atomic positions parameters and site occupancies) were calculated by the full-potential linear muffin-tin orbital (FP-LMTO) method,[22] which is a powerful all-electron technique within the framework of density functional theory for the calculation of different properties of crystalline materials. The space was divided into so-called muffin-tin spheres (MTS) surrounding atomic sites and the interstitial regions between them. No approximations were introduced either for the shape of the charge density and potential inside MTS or in the interstitial region. The basis set, charge density and potential were expanded in spherical harmonic series within nonoverlapping MTS and in Fourier series in the interstitial region. The basis set of augmented linear muffin-tin orbitals was used.[23] The tails of the basis functions outside their parent spheres were linear combinations of Hankel and Neumann functions with nonzero kinetic energy. The basis set included 4s, 4p and 3d orbitals on the sites of transition metal atoms T, and 3d, 4s, 4p and 4d orbitals on the Ga/Zn sites E. All states were contained in the same energy panel. We adopted a double basis in which we used four different orbitals of Hankel and Neumann functions with different kinetic energies. The spherical harmonic expansion of the charge density, potential, and basis functions were carried out up to $l = 6$. The integration over the Brillouin zone was performed by the improved tetrahedron method[24] with 206 irreducible tetrahedra (1296 tetrahedra in the full Brillouin zone). The exchange and correlation potential and energy were treated in the generalised gradient approximation according to Perdew and Wang.[25]

Most conventional methods for the calculation of the electronic structure of crystals, including the FP-LMTO method applied here, were developed for completely ordered compounds. In the case of partially ordered systems such as $T_8Ga_{41-x}Zn_x$, however, one has to deal with atoms of two kinds of elements, Zn and Ga, distributed randomly on some of the sublattices. To handle this problem we applied the so-called virtual-crystal approximation (VCA), which is the simplest approximation in the hierarchy of mean-field approaches[26] and can be easily combined with a full-potential technique. VCA treats a position on the sublattices occupied by Zn or Ga as a fictitious atom with the nuclear charge $Z = xZ_{Zn} + (1-x)Z_{Ga}$ (in which Z_A is the corresponding nuclear charge of the pure element A) and a corresponding number of valence electrons so as to neutralise the charge. The mean-field treatment is sufficient to describe the case of randomly distributed atoms,[26] and in particular it has been shown that VCA is a suitable approximation for calculating the electronic structure of alloys between neighbouring elements in the periodic table.[27]

Acknowledgement

This work was supported by the Swedish National Science Research Council (NFR), the Göran Gustafsson Foundation and the Materials Consortium "ATOMICS". Additionally, we acknowledge a fund from the European Community through its "Access to Research Infrastructure" action of the "Improving Human Potential" Program. S.I.S. thanks J. M. Wills (Los Alamos) for valuable discussions.

[1] H.-J. Flad, F. Schautz, Y. Wang, M. Dolg, A. Savin, *Eur. Phys. J. D* **1999**, *6*, 243.
[2] C. E. Moore, *Atomic Energy Levels*, National Bureau of Standards, Washington DC, **1971**.
[3] U. Häußermann, S. I. Simak, *Phys. Rev. B*, in press.
[4] S. Zhen, K. Seff, *J. Phys. Chem. B* **1999**, *103*, 6493.
[5] Binary intermetallic Zn compounds with Zn–Zn interactions may be divided into systems T_mZn_n (T = earlier transition metal) and A_mZn_n (A = electropositive metal, from the alkali, alkaline earth or lanthanide groups). P. Villars, L. D. Calvert, *Pearsons Handbook of Crystallographic Data for Intermetallic Compounds*, 2nd ed., ASM International: Materials Park, Ohio, USA, **1991**. Usually $n > m$. In the first case, where Zn can be considered to be in the oxidation state zero, Zn atoms form metallic bonded homonuclear networks with high coordination numbers in which T atoms are encapsulated (e.g. $CoZn_{13}$, $RuZn_6$). In the second case (polar intermetallics), Zn is partly reduced and may even form covalently bonded homonuclear networks with low coordination numbers (e.g. as in CaZn, $CaZn_2$).
[6] U. Häußermann, P. Viklund, C. Svensson, S. Eriksson, P. Berastegui, S. Lidin, *Angew. Chem.* **1999**, *111*, 580; *Angew. Chem. Int. Ed.* **1999**, *38*, 488.
[7] K. Girgis, W. Peter, G. Pupp, *Acta Crystallogr. Sect. B* **1975**, *31*, 113.
[8] G. Trambly de Laissardière, D. Nguyen Manh, L. Magaud, J. P. Julien, F. Cyrot-Lackmann, D. Mayou, *Phys. Rev. B* **1995**, *52*, 7920.
[9] R. Ferro, A. Saccone in *Materials Science and Technology*, *Vol. 1*: *The Structure of Solids* (Eds.: R. W. Cahn, P. Haasen, E. J. Kramer), VCH, Weinheim, **1993**, pp. 123–215.
[10] K. Yvon, *Acta Crystallogr. Sect. B* **1975**, *31*, 117.
[11] U. Häußermann, P. Viklund, M. Boström, R. Norrestam, S. I. Simak, *Phys. Rev. B* **2001**, *63*, 125118.
[12] U. Häußermann, M. Boström, P. Viklund, Ö. Rapp, T. Björnängen, unpublished results.
[13] H.-G. Meissner, K. Schubert, *Z. Metallkd.* **1965**, *56*, 475.
[14] P.-E. Werner, *Ark. Kemi* **1969**, *31*, 513.
[15] Siemens Analytical X-ray Instruments Inc., SMART Reference Manual, Madison, Wisconsin, USA, **1996**.
[16] Siemens Analytical X-ray Instruments Inc., ASTRO and SAINT: Data Collection and Processing Software for the SMART System, Madison, Wisconsin, USA, **1995**.
[17] G. M. Sheldrick, SADABS, Program for Scaling and Correction of Area Detector Data, University of Göttingen, Germany, **1996**.
[18] G. M. Sheldrick, SHELXTL Version 5.1, Bruker AXS, Madison, Wisconsin, USA, **1998**.
[19] Rigaku/MSC, Inc. and Prekat AB, *Twin Solve*: *A Program for the Deconvolution and Processing of Rotation Twins*, The Woodlands, Texas, USA, **2001**.
[20] A. C. Larson, R. B. von Dreele, M. Lujan, *GSAS*: *The General Structure Analysis System*; Los Alamos National Laboratory: Los Alamos, USA, **1994**.
[21] H. Hartmann, W. Mässing, *Z. Anorg. Allg. Chem.* **1951**, *266*, 98.
[22] J. M. Wills, O. Eriksson, M. Alouani, D. L. Price in *Electronic Structure and Physical Properties of Solids*: *The Uses of the LMTO Method* (Ed.: H. Dreysse), Springer, Berlin, **2000**, p. 148; J. M. Wills, B. R. Cooper, *Phys. Rev. B* **1987**, *36*, 3809; D. L. Price, B. R. Cooper, *Phys. Rev. B* **1989**, *39*, 4945.
[23] O. K. Andersen, *Phys. Rev. B* **1975**, *12*, 3060.
[24] P. E. Blöchl, O. Jepsen, O. K. Andersen, *Phys. Rev. B* **1994**, *49*, 16223.
[25] J. P. Perdew, Y. Wang, *Phys. Rev. B* **1992**, *45*, 13244.
[26] J. S. Faulkner, *Prog. Mater. Sci.* **1982**, *27*, 3; F. Ducastelle, *Order and Phase Stability in Alloys*, North-Holland, Amsterdam, **1991**.
[27] P. James, I. A. Abrikosov, O. Eriksson, B. Johansson in *Properties of Complex Inorganic Solids* (Eds.: A. Gonis, A. Meike, P. E. A. Turchi), Plenum, New York, **1997**, p. 57; I. A. Abrikosov, P. James, O. Eriksson, P. Söderlind, A. V. Ruban, H. L. Skriver, B. Johansson, *Phys. Rev. B* **1996**, *54*, 3380; U. Häußermann, S. I. Simak, I. A. Abrikosov, B. Johansson, S. Lidin, *J. Am. Chem. Soc.* **1998**, *120*, 10136.
[28] L. M. Gelato, E. Parthé, *J. Appl. Crystallogr.* **1987**, *20*, 139.

Received: May 11, 2001 [F3252]

